

1 NEWTS1.0: Numerical model of coastal Erosion by 2 Waves and Transgressive Scarps

3 Rose V. Palermo^{1,2}, J. Taylor Perron³, Jason M. Soderblom³, Samuel P. D. Birch⁴, Alexander G.
4 Hayes⁵, Andrew D. Ashton⁶

5 ¹ U. S. Geological Survey, St. Petersburg Coastal and Marine Science Center, St. Petersburg, Florida 33701, USA

6 ² MIT-WHOI Joint Program in Oceanography/Applied Ocean Science & Engineering, Cambridge and Woods Hole,
7 MA, USA

8 ³Department of Earth, Atmospheric and Planetary Sciences, Massachusetts Institute of Technology, Cambridge,
9 MA, USA

10 ⁴Department of Earth, Environmental, and Planetary Sciences, Brown University, Providence, RI, USA

11 ⁵Department of Earth, Atmospheric and Planetary Sciences, Cornell University, Cambridge, MA, USA

12 ⁶Department of Geology and Geophysics, Woods Hole Oceanographic Institution, Woods Hole, MA, USA

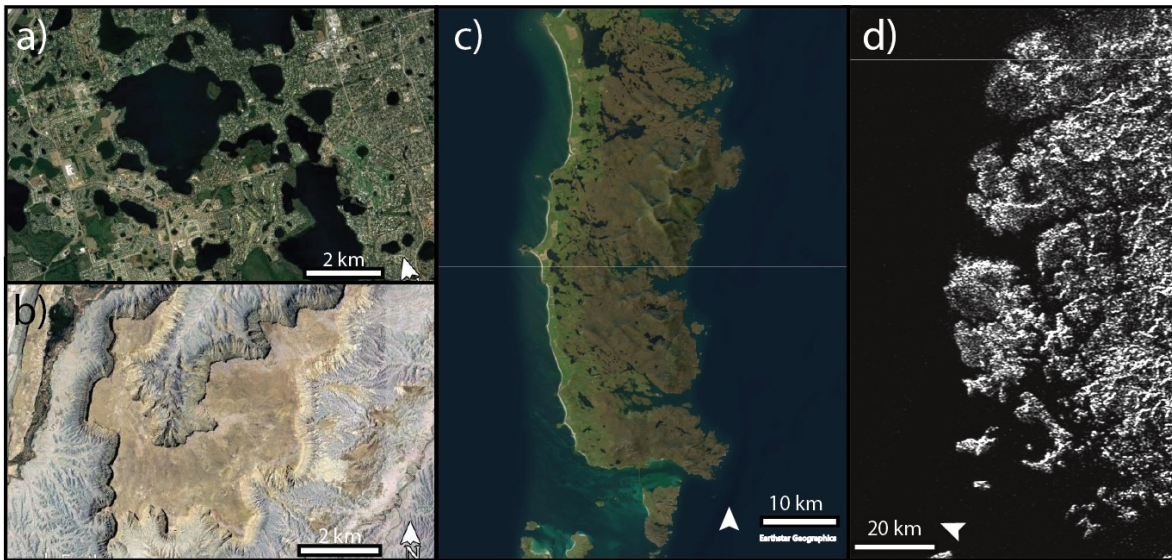
13 *Correspondence to:* Rose V. Palermo (rpalermo@usgs.gov)

14 Abstract: Models of rocky coast erosion help us understand the physical phenomena that control
15 coastal morphology and evolution, infer the processes shaping coasts in remote environments,
16 and evaluate risk from natural hazards and future climate change. Existing models, however, are
17 highly complex, computationally expensive, and depend on many input parameters; this limits
18 our ability to explore planform erosion of rocky coasts over long timescales (100s to 100,000s
19 years) and a range of conditions. In this paper, we present a simplified cellular model of coastline
20 evolution in closed basins through uniform erosion and wave-driven erosion. Uniform erosion is
21 modeled as a constant rate of retreat. Wave erosion is modeled as a function of fetch, the
22 distance over which the wind blows to generate waves, and the angle between the incident wave
23 and the shoreline. This reduced complexity model can be used to evaluate how a detachment-
24 limited coastal landscape reflects climate, sea level history, material properties, and the relative
25 influence of different erosional processes.

26 1 Introduction

27 Rocky coastlines are erosional coastal landforms resulting from the landward
28 transgression of a shoreline through bedrock. They make up approximately 80% of global coasts
29 (Emery and Kuhn, 1980) and often erode slowly through the impact of waves (Adams et al.,
30 2002, 2005), abrasion by sediment (Sunamura, 1976; Robinson, 1977; Walkden & Hall, 2005;
31 Bramante et al., 2020), and chemical weathering (Sunamura, 1992; Trenhaile, 2001). Rocky
32 coastlines protect coastal communities from erosion and flooding, provide sediment for estuaries,
33 marshes, and beaches, serve as important habitats (such as kelp forests), and support tourism
34 economies. The imprint that each erosional mechanism leaves on the shoreline may be further
35 complicated by sea-level changes, accumulation and redistribution of sediment, heterogeneities
36 in the bedrock, or climate forcings. Wave-driven erosion occurs at a rate proportional to the
37 wave power (Huppert et al., 2020). Therefore, over long timescales, waves tend to erode more
38 exposed parts of coastlines preferentially, blunting headlands while preserving the shapes of
39 sheltered embayments. South Uist, Scotland exemplifies this phenomenon, where the west side
40 of the island is open to the Atlantic Ocean and therefore smoother than the east side, which is
41 relatively protected (Fig. 1c). Uniform erosional processes, like dissolution or mass backwasting,
42 erode at a nearly uniform rate everywhere along a coastline and result in smooth, rounded coastal
43 features punctuated by skewed, pointy promontories or headlands (Howard, 1995). Instances of

44 uniform erosion on lakes include dissolution and backwasting occurring on karst lakes found in
45 Florida, USA (Fig. 1a) as well as scarp retreat due to weathering and backwasting occurring on
46 Caineville Mesa, Utah, USA (Fig. 1b).
47



48
49 Figure 1: a) Karst lakes in Florida, USA (Map Data: © Google Earth,
50 Landsat/Copernicus). Lake Butler and the surrounding region. b) Caineville Mesa, Utah, USA
51 (Map Data: © Google Earth, Landsat/Copernicus). c) South Uist, Scotland (Map Data: Esri
52 World Imagery, Earthstar Graphics). d) Cassini synthetic aperture radar (SAR) image of Kraken
53 Mare, Titan (NASA).
54

55 Although the relative influence of uniform erosion processes, such as dissolution, and
56 wave-driven erosion are still being quantified (Trenhaile, 2015), the shape of coastlines may
57 offer a means to infer dominant processes in remote environments where in situ measurements
58 are impractical, such as arctic coasts, where local field data are sparse, or remote planetary
59 bodies, such as Titan (Fig. 1d). A reduced complexity model of long-term, planform evolution of
60 erosion-dominated coasts can provide insights about the importance of wave erosion relative to
61 uniform erosion, such as backwasting of permafrost (Günther et al., 2013). Here, we present a
62 reduced-complexity model of detachment-limited coastal erosion in closed basins, such as lakes
63 or inland seas, by uniform erosion and wave erosion. We test the model by comparing our
64 numerical solution of erosion with an analytical solution and test for model result sensitivity to
65 grid resolution and input parameters. Finally, we describe how this model may be applied
66 beyond closed basins to open coasts and islands (See Section 5).

67 2 Background

68 2.1 Previous Models of Coastal Erosion

69 2.1.1 Models of wave-driven erosion

70 Models of rocky coastline geomorphology have historically focused on the erosion of the
71 cross-shore profile through sea-level rise (Walkden and Hall, 2005; Young et al., 2014), wave

72 impacts (Adams et al., 2002, 2005; Huppert et al., 2020), and the competing effects of sediment
73 abrasion and sediment cover (Kline et al., 2014; Young et al., 2014; Sunamura 2018; Trenhaile,
74 2019). But recent work has explored the alongshore variability (Walkden and Hall, 2005) and
75 planform evolution of these features (Limber & Murray, 2011; Limber et al., 2014; Sunamura,
76 2015; Palermo et al., 2021), with particular focus on either the relationship between planform
77 morphology and retreat rates following storms (Palermo et al., 2021) or the persistence of an
78 equilibrium coastline shape consisting of headlands interspersed with pocket beaches due to
79 variable lithology, grain size, or sediment tools and cover (Trenhaile, 2016; Limber & Murray,
80 2011; Limber et al., 2014).

81 Existing models of planform erosion of rocky beaches include 1) a mesoscale (1 to 100
82 years) alongshore-coupled cross-shore profile model, SCAPE (Walkden and Hall, 2005), in
83 which waves erode the substrate when the substrate is not armored by sediment and sediment is
84 transported by waves using linear wave theory; 2) a numerical model of sea-cliff retreat that
85 focuses on the mechanical abrasion of a notch at the cliff toe and subsequent failure of the cliff
86 and sediment comminution in the surf zone (Kline et al., 2014); and 3) a numerical model of
87 headlands and pocket beaches that takes into account wave energy convergence/divergence and
88 the processes of sediment production and redistribution by waves (Limber et al., 2014).

89 Previous work on marsh-shoreline erosion considers the heterogeneity of substrate
90 erodibility using a percolation theory model (Leonardi & Fagherazzi, 2015). In this system, low
91 wave energy conditions lead to patchy failure of large marsh portions, resulting in a strong
92 dependence on the spatial distribution of substrate resistance. In contrast, high-wave-energy
93 conditions cause the shoreline to erode uniformly, such that the spatial heterogeneity in marsh
94 erodibility does not influence the erosion rate (Leonardi & Fagherazzi, 2015). This ignores
95 variations in fetch, which can be important for rocky coastal systems.

96 These previous process-based models are all computationally expensive and require
97 specific knowledge of sediment and wave characteristics to accurately apply at local scales. To
98 model systems for which minimal field data are available, or to explore the general behavior of
99 planform erosion in rocky coasts under a broad range of conditions, a reduced-complexity model
100 (Ranasinghe, 2020) is necessary.

101 2.1.2 Models of uniform erosion

102 Howard (1995) modeled the retreat of a closed basin scarp as a uniform erosion process.
103 Howard's approach identifies gridded domain points as either interior or exterior to the
104 escarpment and erodes the escarpment edge at a constant rate in all directions originating from
105 adjacent points (Howard, 1995). In his model experiments, the escarpment retreats uniformly
106 toward the interior of the domain from the exterior. This uniform scarp retreat is analogous to
107 coastline retreat in response to dissolution of a uniform substrate. Although Howard's model was
108 designed for a different, subaerial system, the same process law can describe uniform shoreline
109 erosion along the margins of a liquid-filled closed basin, as we assume the planform shoreline
110 also erodes at the same rate in all directions.

111 Shorelines formed by dissolution in karst landscapes have received some attention,
112 mostly in the context of cave collapse features or sinkholes (Johnson, 1997; Martinez et al.,
113 1998, Yechieli et al., 2006). However, most research has focused on the initial formation of these
114 features; studies of the long-term retreat of coastlines due to dissolution are focused on the
115 meter-scale erosion of coastal notches through mechanical and biochemical erosion and by

116 dissolution (Trenhaile 2013; Trenhaile, 2015) and to our knowledge have not been evaluated
117 over a larger spatial scale.
118

119 3 Model

120 We developed the Numerical model of coastal Erosion by Waves and Transgressive
121 Scarps, V1.0 (NEWTS1.0) (Palermo et al., 2023) to study the planform-shoreline erosion of
122 detachment-limited coasts by waves, uniform erosion, or a combination of these processes. This
123 reduced-complexity model can be used to explore long-term (thousands to millions of years)
124 trends in landscape evolution that result from these processes across the appropriate sea- or lake-
125 level change conditions. Uniform erosion includes dissolution or mass backwasting and is
126 modeled with a spatially uniform rate of shoreline retreat, which generally smooths the coastline
127 and generates cusped points where promontories are eroded. Wave erosion occurs in proportion
128 to the wave energy that the coastline is exposed to and to the angle of incidence of the incoming
129 waves, such that the erosion rate depends on the wave energy in the cross-shore direction per
130 unit of length along the coast (Komar, 1997; Ashton & Murray, 2009; Huppert et al., 2020).
131 Coastlines that have larger exposure (larger fetch) experience higher wave energy and therefore
132 faster wave erosion. We model this energy-dependent erosion by computing the fetch of every
133 incident wave angle that may impact a given point on the shoreline and weighting this fetch by
134 the cosine of the angle between the incident wave crests and the shoreline. Mathematically, this
135 is equivalent to the dot product of the direction of wave travel and the direction normal to the
136 shoreline.

137

138 3.1 General description and model setup

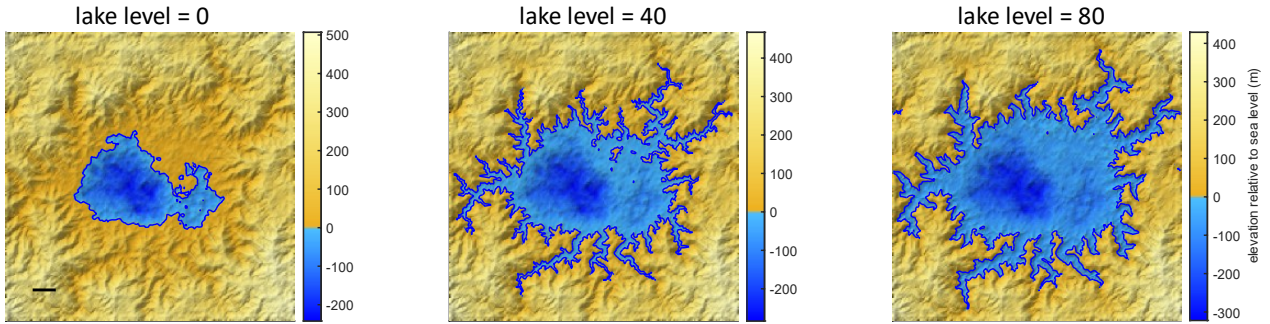
139 3.1.1 Model domain and structure

140 3.1.1.1 Model domain

141 The domain of the model (Fig. 2) is a grid discretized into N_x cells in the x direction and N_y
142 cells in the y direction, with cell spacings Δx and Δy , such that $x_i = i\Delta x$ and $y_j = j\Delta y$. The
143 value of each grid cell, $z_{i,j}$, corresponds to the landscape elevation. The boundaries of the grid
144 are periodic. Each cell in the domain is defined as either liquid or land based on its elevation
145 relative to sea or lake level. The model could apply to lake level in closed basins or sea level in
146 semi-closed seas or open coasts. For simplicity, in this manuscript we will use “lake” to refer to
147 the liquid bodies. “Lake cell” refers to cells occupied by liquid and “lake level” refers to the
148 elevation of the liquid level. Cells below lake level are fixed and do not erode. Shoreline cells,
149 defined as land cells directly adjacent to liquid, may be eroded by coastal processes through
150 uniform erosion and wave erosion. Lake level is an input to the system that the user can vary
151 throughout a model run.

152

153
154



155
156 Figure 2: Example model domain with a lake level of a) 0 m, b) 40 m, and c) 80 m. This domain
157 is used in Figs. 4 and 5.

158 3.1.1.2 Identification of liquid body and shoreline cells

159 Boundaries in the grid are identified using pixel connection definitions of either 4-connected,
160 in which connections occur only across edges, or 8-connected, in which connections occur either
161 across edges or at corners. Liquid cells that are 8-connected to each other comprise the same
162 liquid body. The liquid body could represent a sea or lake, so for simplicity we call a liquid cell a
163 “lake cell” and a liquid body a “lake” in this manuscript. Islands are defined as groups of land
164 cells that are surrounded by liquid cells. Lakes can also occur inside islands and islands inside
165 these lakes, so we define a lake hierarchy to identify and model each lake individually. The first
166 level in this hierarchy is the land that is connected to the border of the domain. First order lakes
167 are lakes that are immediately surrounded by this land that extends to the border of the domain.
168 A first order island is immediately surrounded by a first order lake. A second order lake is
169 surrounded by a first order island, and so on. This continues such that Nth-order islands are
170 surrounded by Nth-order lakes, and Nth-order lakes are surrounded by N-minus-one-order
171 islands. This hierarchy allows us to identify and isolate unique lakes, which will be important
172 when we consider wave-driven erosion.

173

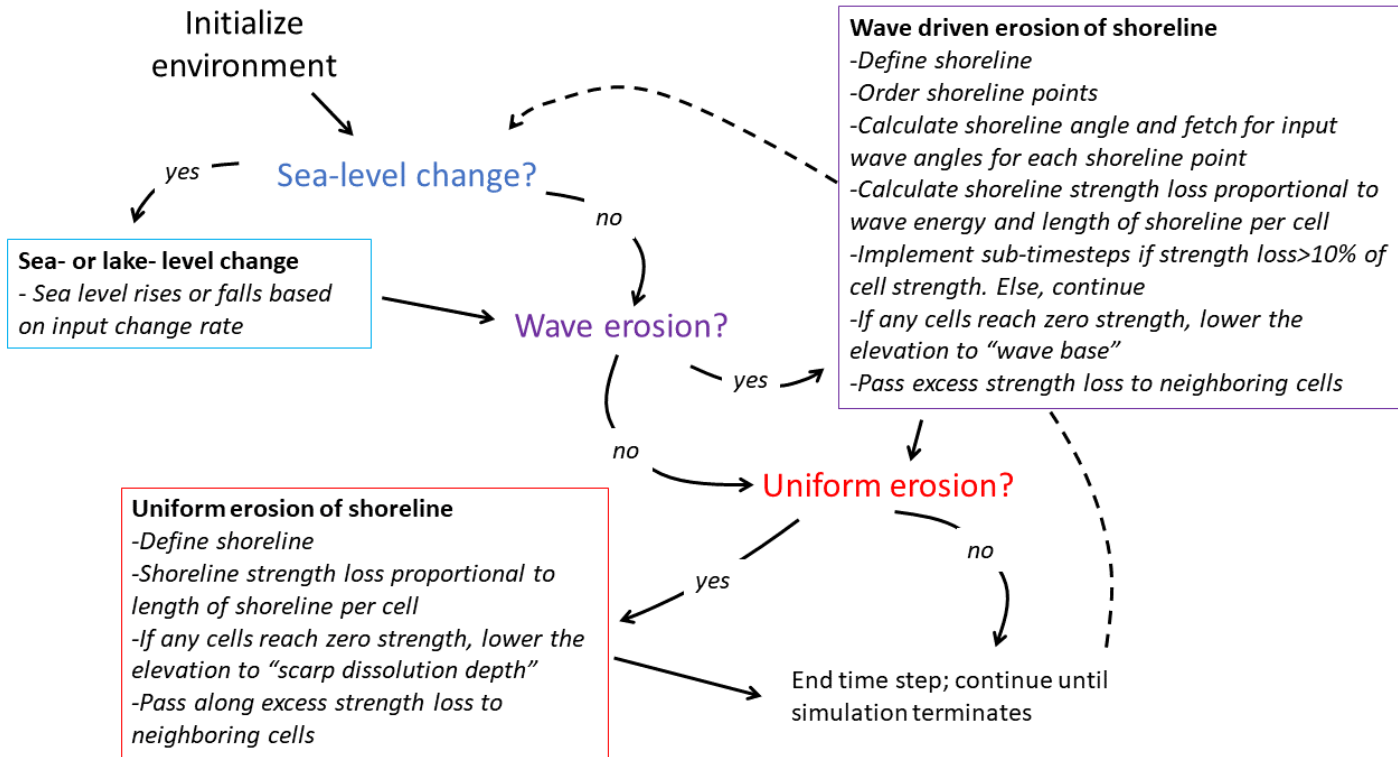
174 3.1.1.3 Cellular grid erosion

175 Each cell starts with an initial strength, S_{init} , (see Sections 3.1.3 to 3.3) which is depleted
176 according to a rate law associated with each coastal process until reaching 0 (see Sections 3.2
177 and 3.3), at which point the cell erodes. Coastal erosion occurs on shoreline cells, defined as land
178 cells adjacent to liquid cells, and decreases the elevation of those cells by a specified depth of
179 erosion, d_e , which is user specified. For cells eroded by coastal processes, $\mathbf{z}(\mathbf{t}) = \mathbf{z}(\mathbf{t} - \mathbf{1}) -$
180 d_e , where \mathbf{t} is model time. For uniform erosion, d_e is conceptualized as the scarp dissolution
181 depth. For wave erosion, is conceptualized as a wave base. Shoreline cells become lake cells
182 once eroded. To avoid numerical artifacts associated with the time discretization, the timestep
183 must be set such that the amount of erosion per iteration is a small fraction of the total cell size.
184 In practice, we set the time step to erode less than $1/10^{\text{th}}$ of a cell at a given time given the cell
185 spacing and rate law. The model run terminates if a lake cell becomes adjacent to a boundary cell
186 because the wave erosion model requires a closed coastline.

187

188 3.1.1.4 Order of operations

189 During each timestep, erosion occurs according to three steps, if enabled: 1) Sea- or lake-
 190 level Change, 2) Wave Erosion, and 3) Uniform Erosion (Fig. 3). Here we describe the general
 191 model components and simulation procedure. The governing equations for Uniform Erosion and
 192 Wave erosion are outlined in more detail in sections 3.2 and 3.3, respectively.
 193



194
 195 Figure 3: Model structure showing the time loop in which the model 1) updates sea- or lake-level
 196 change, then calculates shoreline erosion due to 2) waves and 3) uniform erosion processes.

197
 198 The first operation of the model is lake-level change. The lake level changes as an input rate
 199 or according to an input lake- level curve. The new lake level is used to define the lake(s) and
 200 shoreline(s) (Section 3.1.1.2 and 3.1.2).

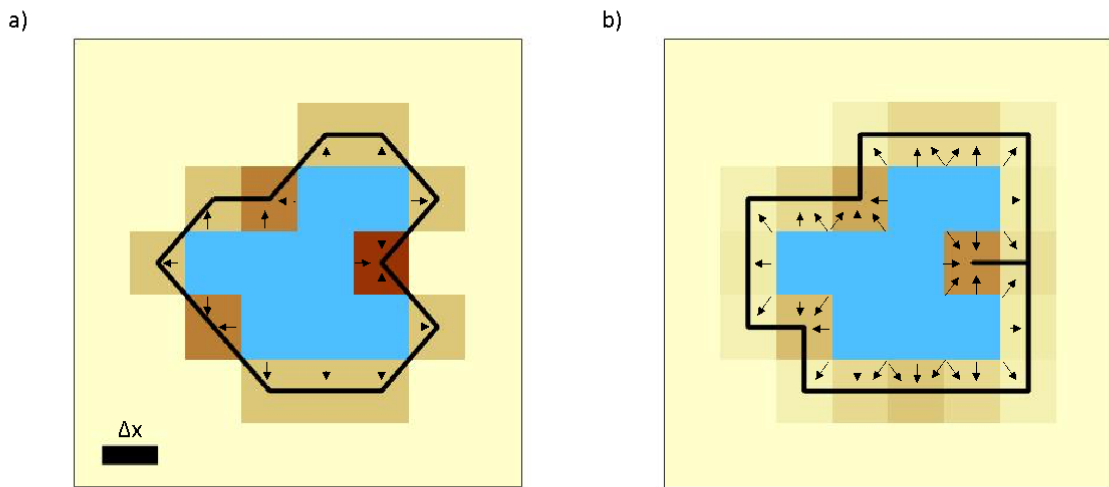
201 Next, wave erosion of the shoreline(s) occurs as a function of the fetch—the open-water
 202 distance wind and waves travel before reaching a point on the coast—and the angle between the
 203 wave crests of the incident waves, φ , and the azimuth of the shoreline, θ (Section 3.3). In this
 204 module, the shoreline is first identified and traced such that shoreline cells are ordered in a
 205 counterclockwise direction. The shoreline is then used to calculate the shoreline angle, incident
 206 wave angle, and associated fetch at each cell along the shoreline (Section 3.3.1). The elevation of
 207 eroded shoreline cells is lowered, their labels are changed to liquid cells as appropriate, and the
 208 shoreline is updated (See Section 3.4, Fig 5). This approach considers sediment removal as
 209 instantaneous. Future variations of the model could consider the erosion also as a function of the
 210 height of the material being eroded or the excavation rate of weathered rubble.

211 Finally, uniform erosion of the updated shoreline occurs (Section 3.2). Here, the shoreline
 212 erodes as a function of the alongshore length of the shoreline as measured along cell boundaries

213 (Section 3.1.2 and 3.2). And again, the elevation of eroded shoreline cells is lowered, the labels
214 of eroded cells are changed to liquid cells, and the shoreline is updated.

215
216 3.1.2 Defining the shoreline

217 There are two options for defining shoreline cells: the 8-connected case, in which
218 successive land cells along the shoreline may border one another either at cell edges or at cell
219 corners (Fig. 4a), or the 4-connected case, in which successive land cells along the shoreline may
220 border one another only at cell edges (Fig. 4b). In the case of an 8-connected shoreline, shoreline
221 cells only border liquid cells at cell edges (Fig. 4a), whereas shoreline cells in a 4-connected
222 shoreline can border liquid cells at cell edges or at cell corners (Fig. 4b). We choose Δx and Δy
223 to be small enough to represent the relevant features of the shoreline. If lake-level change occurs
224 in the simulation, the relevant features in the landscape should be taken into account when
225 choosing Δx and Δy . Here, we present simulations where Δx and Δy are equal. The model can
226 operate with different Δx and Δy ; however, there could be resulting errors which have not been
227 tested.



228
229 Figure 4: Shoreline cells and associated strength loss weighting for a shoreline that is a) 8-
230 connected or b) 4-connected. Arrows point in the direction of erosion into each shoreline cell
231 from neighboring lake cells. Increasing darkness of shoreline cells indicate increasing strength
232 loss weighting.

233 The shoreline cells need to be ordered so that the lake can be represented as a polygon for
234 the fetch computation. To order the shoreline cells in closed loops, we start at the first indexed

235 shoreline cell of the longest shoreline and move counterclockwise to find the next shoreline cell.
236 Once a sequence of the first 3 cells is repeated, the loop is closed and the shoreline is deemed
237 complete. Any remaining shoreline cells that do not lie on this loop represent the shoreline of a
238 separate first-order lake, or of an island or higher order lake contained within the lake. Next,
239 ordering the shorelines of the islands contained within the current lake begins on the first
240 remaining shoreline cell. We repeat this process until all land cells bordering liquid are included
241 in a closed shoreline. When there are multiple first-order lakes in a landscape domain, the
242 shorelines for each lake and its enclosed islands are ordered one at a time.

243 3.1.3 Cell strength and coastal erosion processes

244 All cells start with an initial strength, S_{init} , which represents how difficult it is to erode
245 the land (Equation 1). We model a material of uniform strength in both planform space and
246 elevation across the domain, but this could easily be extended to a scenario with a material of
247 heterogeneous strength across the domain. The strength of a cell is initialized as a reference
248 strength, S_0 , multiplied by the ratio between the cell area, $A = \Delta x \Delta y$, and a reference cell area,
249 $A_0 = \Delta x_0 \Delta y_0$, with reference spacing Δx_0 and Δy_0 (Equation 1). The reference strength and
250 area nondimensionalize strength and maintain proportions that mitigate discretization bias. The
251 magnitude of these values can be chosen by the user.

$$252 \quad S_{init} = S_0 \frac{A}{A_0} \quad (1)$$

253 Strength is lost from each shoreline cell at a rate that depends on the exposed perimeter of
254 the cell and an erosion rate law specific to either uniform erosion or wave erosion processes.
255 Change in strength is grid-independent for grids sufficiently fine to satisfy model stability
256 because the strength is initialized with a reference cell area in proportion to the parameterized
257 cell area. To mitigate discretization bias, Δx , Δy , and Δt must be sufficiently small that Δt is less
258 than the time to completely erode a cell (See Sections 3.2 and 3.3), and that Δx and Δy properly
259 represent the shoreline morphology. In practice, we choose Δx to be equal to Δy .

260 As time progresses, each shoreline cell loses strength until failure, $S_{i,j} = 0$, at which
261 point the cell has eroded. It is possible for the strength loss in one time step to exceed the
262 remaining strength of the cell. When this occurs, the excess time spent eroding the cell is passed
263 along to all new shoreline neighbors of the eroded cell, representing the time of erosion that
264 neighboring cell will incur after the erosion of the original shoreline. If a new shoreline cell is
265 inheriting excess time from multiple neighbors, the mean excess time is used to compute the
266 strength loss. In our simulations, taking the mean of the excess time resulted in the least grid
267 bias.

268 Modeled erosion could be underestimated or redistributed improperly if the strength loss
269 for an eroding cell is consistently large relative to the initial strength of the domain. The
270 shoreline would then not update with the newly exposed cells, rather constantly passing strength
271 loss to its neighbors, and inaccurately characterizing the morphology. We implement a sub-
272 timestep routine to capture the effect of the changing shoreline within a single timestep when the
273 strength loss of any shoreline cell in the domain exceeds a certain threshold of the initial
274 strength, α , which ranges between 0 and 1. In the modified time-step routine, the damage is
275 computed and the shoreline updated in sub-timesteps, which segments the time-step and allows
276 erosion to occur in smaller increments.

277 3.2 Uniform erosion model

278 The rate of shoreline retreat by uniform erosion is set by an erodibility coefficient,
 279 $k_{uniform}$ (Eq. 2). Strength loss due to uniform erosion occurs as a function of the amount of
 280 shoreline in contact with the lake for a given cell, represented as the number of 4-connected
 281 sides, and 8-connected corners, c , in contact with lake cells (Eq. 3; Fig. 4). Because the diagonal
 282 of the cell is longer than the side by a factor of $\sqrt{2}$, it would take $\sqrt{2}$ times longer for a shoreline
 283 to retreat across a cell diagonal than in the perpendicular direction. To correct for this in our
 284 model, the strength loss computed from an exposed corner is $\sqrt{2}/2$ as much as the strength lost
 285 from an exposed side.

$$286 \quad \frac{dx}{dt} = k_{uniform}, \quad (2)$$

$$287 \quad \frac{\Delta S_{i,j}}{S_0} = -k_{uniform} \left(s_c + \frac{\sqrt{2}c}{2} \right) \frac{\Delta x}{\Delta x_0} \Delta t, \quad (3)$$

288 3.3 Wave erosion model

289 Wave erosion occurs at a rate determined by a wave erodibility coefficient, k_{wave} [$\text{m}\cdot\text{yr}^{-1}$],
 290 and the wave energy in the cross-shore direction, E (Eq. 4). The wave energy depends on the
 291 wave height, H , and the angle between the wave crests of the incident waves, φ , and the azimuth
 292 of the shoreline, θ (Eq. 5). Wave height scales with fetch, F , such that $H \propto \sqrt{F}$ (Hasslemann,
 293 1973; Smith and Waseda, 2008). Therefore, we use fetch to approximate the wave energy
 294 density for a wave from a given direction on a coastline (Eq. 6). The use of wave energy implies
 295 the assumption of single-period waves.

$$296 \quad \frac{dx}{dt} = k_{wave} E, \quad (4)$$

$$297 \quad E = \frac{1}{16} \rho g H^2 \cos(\varphi - \theta), \quad (5)$$

$$298 \quad E \propto \rho g F \cos(\varphi - \theta), \quad (6)$$

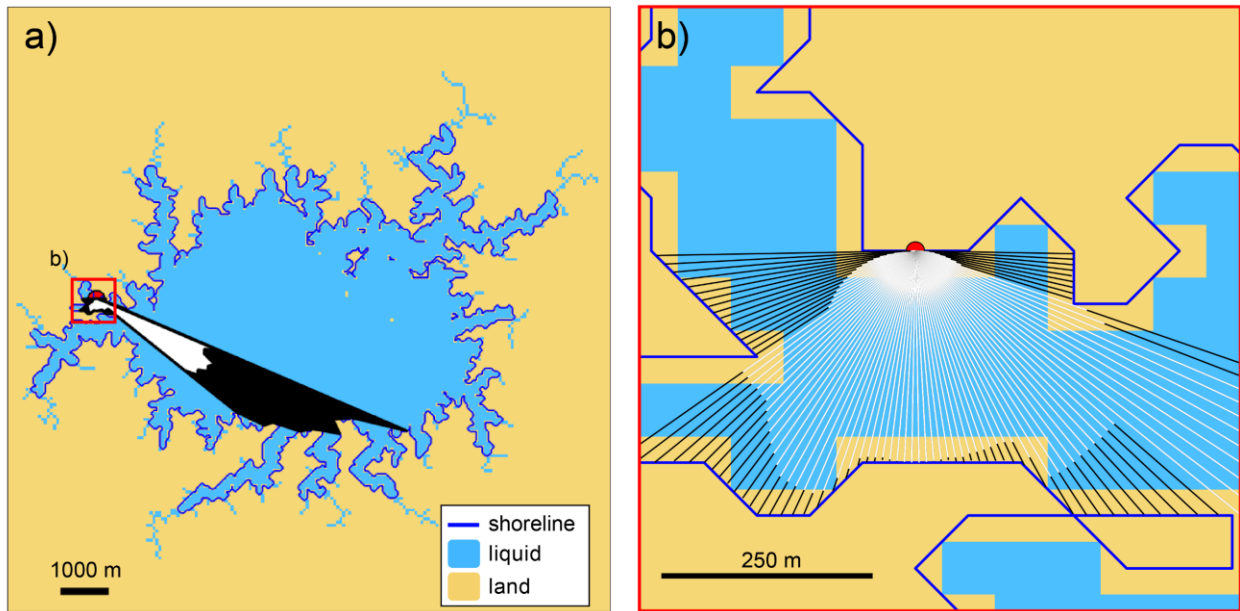
299 The strength loss of a cell due to waves can be described as

$$300 \quad \frac{\Delta S_{i,j}}{S_0} = -k_{wave} \left(s_c + \frac{\sqrt{2}c}{2} \right) \int_{\varphi=0}^{2\pi} F(\varphi) \cos(\varphi - \theta) d\varphi \frac{\Delta x}{\Delta x_0} \Delta t. \quad (7)$$

301 If the strength loss in a time step exceeds a parameter-set threshold, a sub-timestep
 302 routine is implemented. Because the fetch calculation is the costliest step of the model, in this
 303 sub-timestep routine, we estimate the fetch weighting by interpolating the fetch of the nearest
 304 neighbor shoreline cells. This avoids additional costly fetch computations during the sub-
 305 timestep updates and allows us to approximate erosion driven by waves in a way that limits error
 306 without slowing down the model simulation.

307 3.3.1 Modeling wave energy density

308 The rate of strength loss of each shoreline cell is proportional to the wave energy density.
 309 We model the wave energy density to be proportional to the fetch and the cosine of the angle
 310 between the incident wave crest and the shoreline (Fig. 5). To compute this quantity, we measure
 311 the fetch in all directions around the shoreline, in increments of $d\varphi$, for each shoreline cell. For
 312 each direction, we extend a ray from the cell center in the direction $90^\circ - \varphi$ and step along the
 313 ray in increments of a distance δ until reaching the opposite shore. The modeling approach
 314 presented here does not consider the effects of shoaling or refraction, so waves that would
 315 approach the shoreline from beyond 90° are not considered. When the ray extends past the
 316 opposite shoreline, we take one step back and define this point as the intersection. The distance
 317 between this intersection and the originating shoreline cell center is the fetch in the direction
 318 from which a wave would propagate (Fig 4b). The length of fetch may be truncated at an input
 319 maximum length which would represent the distance at which waves saturate and do not
 320 continue to grow. To calculate the amount of strength loss each cell incurs, we compute the area
 321 of a polygon defined by the ray-shoreline intersections for that cell (Fig. 5a). We call this area
 322 the “fetch area.” The length of the ray in each direction is then weighted by the cosine of the
 323 angle between the shoreline and the incident wave crest, $\varphi - \theta$ (Fig. 5a). The area of the polygon
 324 defined by these cosine-weighted fetch lengths is computed and called the “wave area.” The
 325 wave area for each point on the shoreline approximates the integral in Eq. 7.



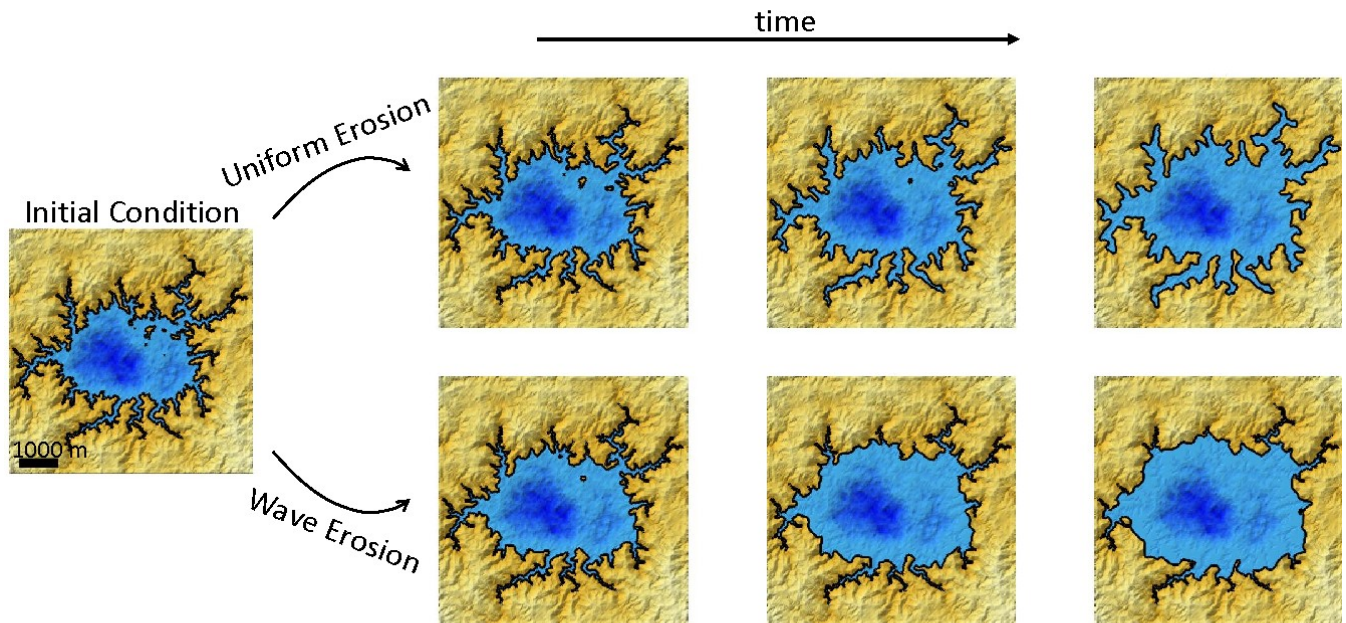
326
 327 Figure 5: a) Fetch area (black) and wave area (white) computed for a point (red circle) on a
 328 typical model shoreline (blue). The area shown in b) is outlined in red. b) Zoomed-in view of
 329 fetch line-of-sight rays (black) and angle-weighted line-of-sight rays (white) computed for the
 330 same point. In this example, $d\varphi = 2^\circ$ and the ray step size, $\delta = 0.05$ m.

331 3.4 Model output

332 The model can be initialized with any user defined topographic model. In the simulations
 333 presented here, we initialize the grid with a synthetic topography consisting of a pseudo-fractal
 334 surface with variance of 10,000 superimposed on an elliptical depression with a depth of 25% of

335 the domain relief and eroded by river incision to 95% of the initial terrain relief using a
 336 landscape evolution model (Perron et al., 2008, 2009, 2012). We then flood the domain by
 337 raising lake level by 40 m. The model of shoreline retreat by uniform and wave erosion is then
 338 applied to the domain. Here, we show examples of an initial landscape eroded by either wave
 339 erosion or uniform erosion, to illustrate separately the effects of the two erosional mechanisms in
 340 the model (Fig. 6). However, all model components may be run in combination. We do not
 341 provide examples of combined uniform and wave erosion models here.

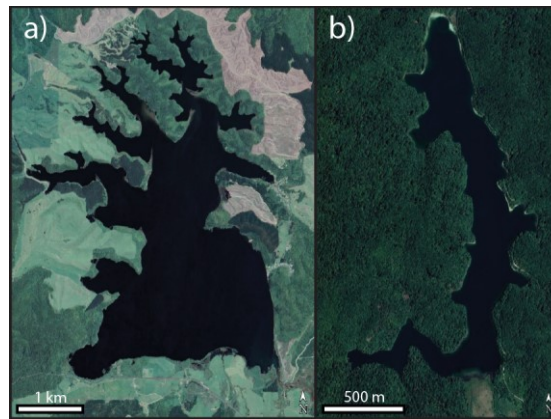
342 The initial shoreline exhibits a dendritic shape due to flooding of the incised river valleys
 343 (Fig. 6). Through time, the uniform erosion model drives shoreline retreat at the same rate
 344 everywhere around the perimeter of the lake, resulting in widening valleys and increasing the
 345 pointedness of promontories or headlands (Fig. 6). The overall shape of the lake is maintained,
 346 but becomes smoother and tends toward circular. In the case of wave erosion, the river valleys
 347 erode slowly while the exposed parts of the coast erode more rapidly (Fig. 6). The embayed river
 348 valleys largely maintain their shapes, whereas the central, high-fetch portion of the coast grows
 349 larger and smoother.



350 Figure 6: Shaded relief maps of example model simulations of uniform erosion and wave erosion
 351 through time, starting from the same initial condition. Blue color indicates liquid cells, with
 352 darker blues indicating deeper depths. Gold color indicates land cells, with lighter shades
 353 indicating higher elevations. Black lines trace shorelines. Erodibility coefficients are $k_{wave} =$
 354 $k_{uniform} = 0.00001 \text{ m}\cdot\text{yr}^{-1}$. Uniform erosion (top) results in greater overall smoothness that is
 355 punctuated by pointy headlands, whereas wave erosion (bottom) results in blunted headlands,
 356 smooth open sections of coast, and preservation of sharp features in sheltered areas. Landscape
 357 time-steps shown correspond to similar amounts of erosion between wave and uniform
 358 examples. The shoreline is defined as 4-connected in these examples.

360 To test our model performance, we compare the planform morphologies of model output
 361 with example shorelines that have known geomorphic processes. While long term coastal cliff
 362 retreat rates could be determined using dating techniques at local field sites (Hurst et al., 2016;
 363 Bossis et al., 2024), more detailed testing of the model would require recreation of plan-view
 364 shape at a broader scale. Because long-term changes in planform morphology during retreat of
 365 bedrock coastlines are generally too slow to be measurable with historical aerial and satellite
 366 images, the data needed to fully validate this model are not presently available. Nonetheless, a
 367 visual comparison can be drawn between coastal features found on Earth and the coastline
 368 shapes generated by each end-member erosional mechanism in the model, which is the main goal
 369 of our modeling approach. These shorelines exhibit the same overall smoothness, punctuated by
 370 sharp headlands, as is seen in the shorelines formed by uniform erosion in our model (Fig. 6).
 371 Although it is beyond the scope of this paper, output from this model could be used to
 372 quantitatively describe shoreline morphologic differences driven by wave and uniform erosional
 373 processes or signatures of sea- or lake- level changes.

374 A bedrock lake that has been eroded recently by waves is exemplified by Lake Rotoehu,
 375 New Zealand (Fig. 7c). In these examples, we observe blunted headlands and smooth, rounded
 376 stretches in open sections of coast, and crenulated shorelines in more protected areas of coast –
 377 similar to the shorelines formed by wave erosion in our model (Fig. 6).
 378
 379



380
 381 Figure 7: a) Lake Rotoehu, New Zealand (Map Data: © Google Earth, CNS/Airbus). b) Plitvice
 382 Lakes, Croatia (Map Data: © Google Earth, DigitalGlobe).

383 4 Model tests

384 4.1 Comparison with analytical solution and sensitivity to shoreline connectedness

385 For the simple case of an initially circular shoreline, we compute the shoreline evolution
 386 analytically and compare this known solution with our numerical model results. For the uniform
 387 erosion case, the rate at which the radius of a circle increases, \dot{r} , is equal to the constant of
 388 erosion, in this case $k_{uniform}$.

$$389 \quad \dot{r}(t) = k_{uniform} \quad (8)$$

390 Therefore, the radius, r , at time, t , and initial radius, r_0 , for uniform erosion is:

391
$$r(t) = r_0 + k_{uniform}t \quad (9)$$

392 For wave erosion, the rate of increase of the radius, \dot{r} , depends on the constant of erosion, k_{wave} ,
 393 and the integral of the fetch, F , at each angle between the incoming wave crest and the shoreline,
 394 $(\varphi - \theta)$ in all directions around the circle:

395
$$F(\varphi) = r\sqrt{2(1 + \cos(2(\varphi - \theta)))} \quad (10)$$

396
$$\dot{r}(t) = \frac{k_{wave}}{2} \int_{-\frac{\pi}{2}}^{\frac{\pi}{2}} (F(\varphi)\cos(\varphi - \theta))^2 d\varphi \quad (11)$$

397 Computing this integral simplifies to:

398
$$\dot{r}(t) = k_{wave} \frac{3\pi}{4} r(t)^2 \quad (12)$$

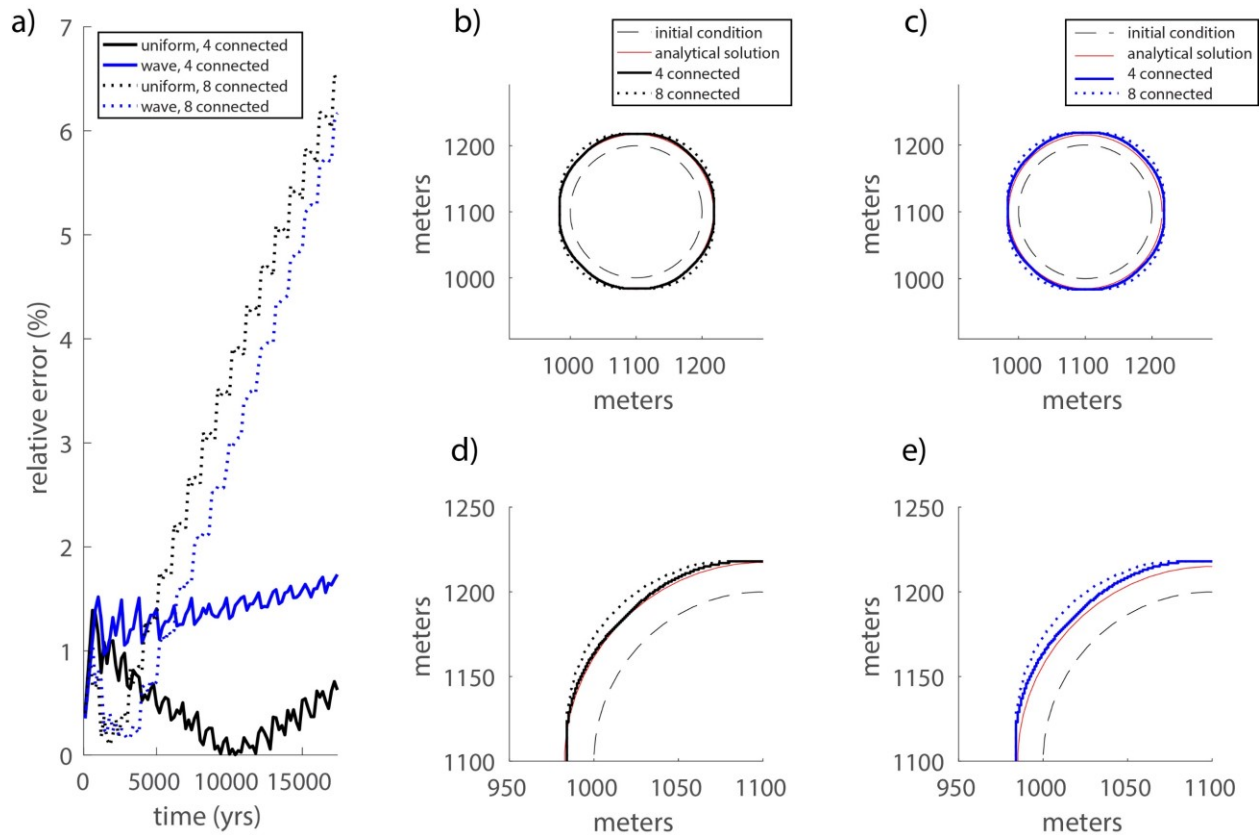
399 Therefore, the radius, r , at time, t , for wave erosion is:

400
$$r(t) = \frac{r_0}{1 - r_0 k_{wave} \frac{3\pi}{4} t} \quad (13)$$

401 We use the analytical solution for the radius through time for each case to calculate the
 402 shoreline position and area of the circular lake as it is eroded by either uniform or wave erosion.
 403 To compute the relative error of the numerical model, a test circular lake is eroded for 17,400
 404 years, resulting in approximately 20% and 25% increase in lake area for wave and uniform
 405 erosion, respectively, and compare this to the analytical solution.

406 Because the model operates on a rectangular grid, some amount of distortion of a circle is
 407 expected. While this distortion cannot be avoided entirely by increasing the grid resolution,
 408 increasing it can reduce the error in the shoreline shape by allowing the shoreline to retreat in
 409 finer increments. A fine grid, however, comes at increased computational cost. The spatial
 410 resolution, Δx and Δy , should be chosen to be small enough to represent the features of the
 411 shoreline, but large enough to keep computational costs reasonable.

412 We perform these simulations for uniform and wave erosion with both 4-connected and
 413 8-connected versions of the model (Fig. 4). The 4-connected model performs significantly better
 414 than the 8-connected model, as shown by the relative error in lake area. The 4-connected case
 415 maintains relative error less than 2% throughout the simulation whereas the error in the 8-
 416 connected model increases roughly linearly with time, ending at approximately 7% (Fig. 8a). The
 417 distortion is worse in the 8-connected case for both uniform erosion and wave erosion, and
 418 systematically worse in the diagonal directions (Fig. 8b,c). This analysis suggests that grid bias is
 419 a more important source of error in the model than spatial discretization.



420

421 Figure 8: a) The error in lake area through time of an initially circular lake relative to the
 422 analytical solution for 4-connected (solid) and 8-connected (dotted) models of uniform erosion
 423 (black) and wave erosion (blue). The initial condition (dashed), analytical solution (red), and
 424 modeled 4-connected and 8-connected shorelines at time=17400 are shown for b) uniform
 425 erosion and c) wave erosion, with zoomed in results shown for d) uniform erosion and e) wave
 426 erosion.

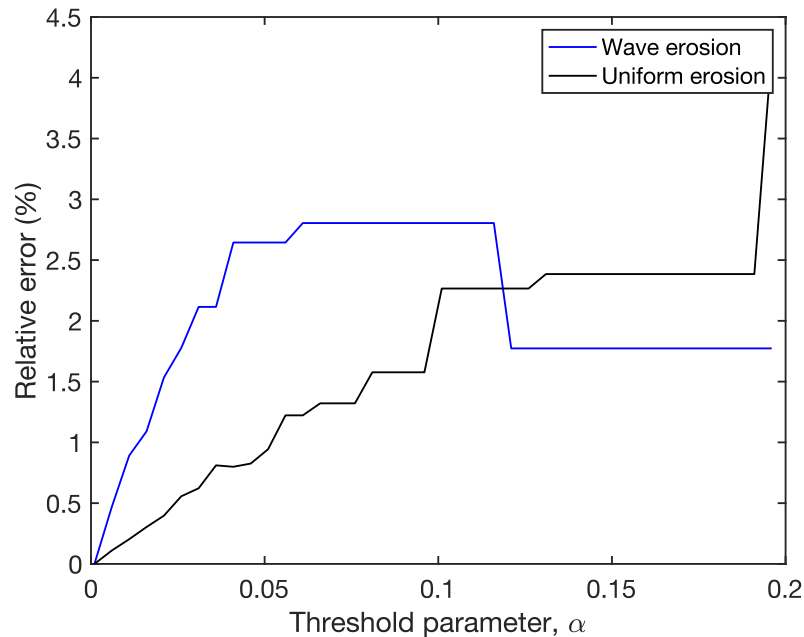
427 4.2 Resolution sensitivity

428 4.2.1 Grid resolution

429 Although the grid resolution affects the size of the features that can be resolved in the
 430 landscape, it does not substantially affect the amount of coastal erosion. As discussed above, the
 431 strength loss in this model is insensitive to grid resolution, Δx , and time step, Δt , assuming that
 432 Δx is fine enough to resolve the features of interest and that Δt is small enough to limit erosion
 433 to less than the maximum cell strength in a single time step. The total amount of strength in the
 434 domain is independent of Δx because the number of cells is proportional to Δx^{-2} and the
 435 strength of each cell is proportional to Δx^2 . The damage in each time step is independent of Δx
 436 because the number of cells on the shoreline is proportional to Δx^{-1} and the damage per cell is
 437 proportional to Δx .

438 4.2.2 Threshold strength parameter

439 The threshold strength parameter, α , was introduced to prevent excess strength reduction
 440 from being neglected when a cell has less strength than is depleted in a timestep. A smaller
 441 threshold strength parameter results in a more frequent application of the sub-timestep routine
 442 and smaller sub-timesteps. With a less stringent threshold strength parameter (>0.05), the
 443 shoreline may erode more than the analytical solution in a time step, leading to a positive slope
 444 in the relative error in strength against the threshold strength parameter (Fig. 9).

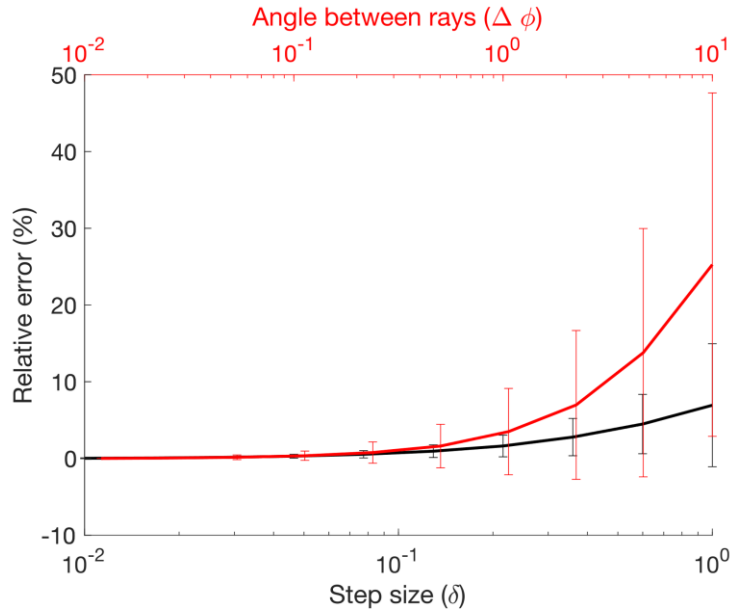


445
 446 Figure 9: Error in total strength reduction as a function of the threshold strength parameter,
 447 expressed as a percentage of the error for the smallest value of the threshold strength parameter,
 448 for the initial condition in Fig. 6 eroded over one time step by uniform erosion (black) and wave
 449 erosion (blue).

450 4.3 Fetch ray angular and distance increments

451 We test the sensitivity of the fetch-area calculation to the angle between rays, $d\phi$, and the
 452 ray step size, δ . This test allows us to analyze the error in fetch of a typical model due to these
 453 parameters. The error measurements provide a basis for selecting an angle between rays and a
 454 ray step size that optimize the trade between computational time and model accuracy.

455 We compute the error in fetch area over a range of ray angles and step sizes. With a fixed
 456 ray step size of $0.05\Delta x$ (the nominal step sized used in our simulations), we compute the fetch
 457 error for each shoreline cell over a range of 0.012° to 10° , corresponding to 30,000 and 36 rays,
 458 respectively. With a fixed ray angle of 2° (the nominal ray angle used in our simulations), we
 459 compute the relative fetch error over a range of ray step sizes between $0.01\Delta x$ to Δx . The fetch-
 460 area error of each cell is computed relative to the fetch area of the finest resolution in each
 461 parameter: 2° between rays and a ray step size of $0.05\Delta x$ (Fig. 10). The error, as well as the
 462 standard deviation in errors, in each scenario converges to zero, indicating that as the angle
 463 between rays and the ray step size become small the fetch area converges to a constant value.



464
 465 Figure 10: Relative error in fetch area for a range of step sizes with ray angle of 2° (black) and
 466 for a range of ray angles with step size of $0.05\Delta x$ (red).

467 5 Discussion and Conclusions

468 In this paper, we present NEWTS1.0, a cellular model of coastline erosion in detachment-
 469 limited environments by uniform erosion and by wave erosion. For uniform erosion, the
 470 coastline erodes at a constant rate everywhere along the shoreline. For wave-driven erosion, the
 471 coastline erodes as a function of the fetch and the angle between the incident waves and the
 472 shoreline.

473 While our uniform erosion rate law is similar to that of Howard (1995), our modeling
 474 approach is different. Because there are multiple mechanisms that may erode a coast in our
 475 model, memory of the strength loss of the substrate is necessary. Rather than rays extending at a
 476 constant rate from the interior points representing retreat as is done in Howard's 1995 model, the
 477 strength of shoreline (or scarp edge) points is reduced by an amount proportional to the number
 478 and direction of neighboring lake cells.

479 Our wave erosion model contains a dependence on wave energy like in other models
 480 (Walkden and Hall, 2005; Limber et al., 2014), but simplifies the influence of sediment and other
 481 factors to a constant. This simplification is useful for locations without readily available grain
 482 size or sediment cover data, and to investigate the long-term influence of these processes.
 483 However, a limitation of this simplified approach is the implicit assumption of a single wave
 484 period when using wave energy rather than wave power in the wave erosion rate law (Equations
 485 4-6). Future work could extend the capabilities to include consideration of wave period.

486 Our model is also unusual among coastal erosion models in that it evaluates multiple
 487 closed coastlines (or lakes) in a landscape domain rather than a single reach of open coastline,
 488 and that it focuses on the planform morphology of eroding rocky closed-basin shorelines. A
 489 limitation of this model is that sediment redistribution is not included in the erosion rate laws and
 490 there is no sedimentation along the coast. Sediment abrasion and cover could be incorporated in
 491 future versions of our model through a spatially heterogeneous and time-dependent erodibility
 492 coefficient, k ; however, this would likely require parameterization from field data.

493 While this model is currently configured to simulate the erosion of closed basins, such as
494 lakes or inland seas, modifications could be made to evaluate open stretches of coast. The two
495 model algorithms that would need to be considered are the routines to order the shoreline and to
496 compute fetch. The routine to order the shoreline requires that the shoreline be a closed loop. To
497 evaluate an open stretch of coast in the model, either the landscape domain could be modified to
498 artificially enclose the open coast or the boundary conditions. The simpler approach is to modify
499 the landscape domain such that an artificial and large basin was made surrounding the domain,
500 identifying these as fixed points that do not erode, and making sure the modified landscape is
501 further than the fetch saturation length from the shoreline of interest. To evaluate an ocean
502 island, enclose it in land beyond the fetch saturation length in distance from the island. If the
503 domain is modified such that the shoreline is a closed loop, all routines should function
504 appropriately. However, if a different routine to order the shoreline is used, the fetch
505 computation would need to be slightly modified. Currently, fetch is computed as an extended ray
506 from a shoreline cell that advances at some interval length until it reaches land and allows for a
507 fetch threshold at some length of wave saturation (See Section 3.3.1). The truncation of
508 computed fetch at the threshold length is implemented following the calculation of the fetch
509 length. If there isn't land on the opposite side of the ray, an error would occur. Therefore, by
510 truncating the fetch length as the ray is extending rather than after the opposite land is found,
511 fetch could be calculated for open coasts. A more complicated, but preferable approach would be
512 to change the boundary conditions. If the boundaries of the open stretch of coast were periodic in
513 the alongshore direction, the entire coast could retreat without introducing an artificial boundary
514 edge and a larger domain. If a fetch vector went off the periodic boundary, it would wrap around
515 to the other side and continue. If a periodic boundary condition is deemed inappropriate for a
516 specific model task, mirrored boundaries in the alongshore direction could be used instead. The
517 shape of the coast would be reflected in each boundary, and fetch vectors would reflect off the
518 boundary.

519 As a reduced-complexity model, NEWTS1.0 can be applied to investigate coastal
520 systems in remote environments where field work is difficult or impossible. This includes
521 locations such as the arctic or Saturn's moon Titan, home to the only other active coastlines in
522 our solar system. The simplicity of our model allows for efficient, long-term simulations of
523 coupled landscape evolution and coastal erosion in detachment-limited systems. Among coastal
524 systems on Earth, investigations of fetch dependence and the resulting morphology given a
525 combination of erosional mechanisms would be particularly relevant to the carbonate
526 geomorphology community, as dissolution and wave activity are both often acting
527 simultaneously along these coasts.

528 **Acknowledgments**

530 We thank David Mohrig, Di Jin, Heidi Nepf, Jorge Lorenzo-Trueba, Santiago Benavides,
531 and Paul Corlies for helpful discussions. We also thank Daniel Ciarletta, Eli Lazarus, and
532 Luca Malatesta for constructive reviews. Any use of trade, firm, or product names is for
533 descriptive purposes only and does not imply endorsement by the U.S. Government.

534 **Funding:**

535 National Science Foundation Graduate Research Fellowship grant 1745302 (RVP)
536 NASA Cassini Data Analysis Program grants 80NSSC18K1057 and 80NSSC20K0484
537 (RVP, JTP, ADA, JMS, SPDB, AGH).
538

539 United States Geological Survey, Coastal and Marine Hazards Research Program (RVP)
540 Heising-Simons Foundation (SPDB)

541

542 **Author contributions:**

543 Conceptualization: RVP, JTP, ADA, JMS, SPDB, AGH

544 Methodology: RVP, JTP, ADA, JMS

545 Investigation: RVP, JTP, ADA

546 Visualization: RVP

547 Supervision: JTP, ADA, AGH

548 Writing—original draft: RVP

549 Writing—review & editing: RVP, JTP, ADA, JMS, SPDB, AGH

550

551 **Competing interests:** Authors declare that they have no competing interests.

552

553 **Code/Data availability:** NEWTS1.0 model (Palermo et al., 2023) code is available at

554 <https://doi.org/10.5066/P9Q6GDGP>.

555

556

557 **6 References**

558 Adams, P. N.: Assessing coastal wave energy and the geomorphic evolution of rocky coasts,
559 University of California, Santa Cruz, 2004.

560 Adams, P. N., Anderson, R. S., and Revenaugh, J.: Microseismic measurement of wave-energy
561 delivery to a rocky coast, *Geol*, 30, 895, [https://doi.org/10.1130/0091-](https://doi.org/10.1130/0091-7613(2002)030<0895:MMOWED>2.0.CO;2)
562 [7613\(2002\)030<0895:MMOWED>2.0.CO;2](https://doi.org/10.1130/0091-7613(2002)030<0895:MMOWED>2.0.CO;2), 2002.

563 Adams, P. N., Storlazzi, C. D., and Anderson, R. S.: Nearshore wave-induced cyclical flexing of
564 sea cliffs, *J. Geophys. Res.*, 110, 2004JF000217, <https://doi.org/10.1029/2004JF000217>,
565 2005.

566 Ashton, A. D., Murray, A. B., Littlewood, R., Lewis, D. A., and Hong, P.: Fetch-limited self-
567 organization of elongate water bodies, *Geology*, 37, 187–190,
568 <https://doi.org/10.1130/G25299A.1>, 2009.

569 Bossis, R., Regard, V., Carretier, S., and Choy, S.: Evidence of slow millennial cliff retreat rates
570 using cosmogenic nuclides in coastal colluvium, *Physical: Geomorphology (including all*
571 *aspects of fluvial, coastal, aeolian, hillslope and glacial geomorphology)*,
572 <https://doi.org/10.5194/egusphere-2023-3020>, 2024.

573 Bramante, J. F., Perron, J. T., Ashton, A. D., and Donnelly, J. P.: Experimental quantification of
574 bedrock abrasion under oscillatory flow, *Geology*, 48, 541–545,
575 <https://doi.org/10.1130/G47089.1>, 2020.

576 Emery, K. O. and Kuhn, G. G.: Erosion of rock shores at La Jolla, California, *Marine Geology*,
577 37, 197–208, [https://doi.org/10.1016/0025-3227\(80\)90101-2](https://doi.org/10.1016/0025-3227(80)90101-2), 1980.

578 Esri. "Imagery" [basemap]. 1:365,662. "World Imagery". January 18, 2024.
579 <https://www.arcgis.com/home/item.html?id=10df2279f9684e4a9f6a7f08febac2a9>. (Jan
580 31, 2024).

581 Günther, F., Overduin, P. P., Sandakov, A. V., Grosse, G., and Grigoriev, M. N.: Short- and
582 long-term thermo-erosion of ice-rich permafrost coasts in the Laptev Sea region,
583 *Biogeosciences*, 10, 4297–4318, <https://doi.org/10.5194/bg-10-4297-2013>, 2013.

584 Hasselmann, K., Barnett, T. P., Bouws, E., Carlson, H., Cartwright, D. E., Enke, K., Ewing, J.,
585 Gienapp, A., Hasselmann, D., and Kruseman, P.: Measurements of wind-wave growth
586 and swell decay during the Joint North Sea Wave Project (JONSWAP)., *Ergaenzungsheft*
587 *zur Deutschen Hydrographischen Zeitschrift, Reihe A*, 1973.

588 Howard, A. D.: Simulation modeling and statistical classification of escarpment planforms,
589 *Geomorphology*, 1995.

590 Huppert, K. L., Perron, J. T., and Ashton, A. D.: The influence of wave power on bedrock sea-
591 cliff erosion in the Hawaiian Islands, *Geology*, 48, 499–503,
592 <https://doi.org/10.1130/G47113.1>, 2020.

593 Hurst, M. D., Rood, D. H., Ellis, M. A., Anderson, R. S., and Dornbusch, U.: Recent acceleration
594 in coastal cliff retreat rates on the south coast of Great Britain, *Proc. Natl. Acad. Sci.*
595 *U.S.A.*, 113, 13336–13341, <https://doi.org/10.1073/pnas.1613044113>, 2016.

596 Kline, S. W., Adams, P. N., and Limber, P. W.: The unsteady nature of sea cliff retreat due to
597 mechanical abrasion, failure and comminution feedbacks, *Geomorphology*, 219, 53–67,
598 <https://doi.org/10.1016/j.geomorph.2014.03.037>, 2014.

599 Komar, P. D.: *Beach processes and sedimentation.*, 1977.

600 Lamont-Smith, T. and Waseda, T.: Wind Wave Growth at Short Fetch, *Journal of Physical*
601 *Oceanography*, 38, 1597–1606, <https://doi.org/10.1175/2007JPO3712.1>, 2008.

602 Limber, P. W. and Murray, A. B.: Beach and sea-cliff dynamics as a driver of long-term rocky
603 coastline evolution and stability, *Geology*, 39, 1147–1150,
604 <https://doi.org/10.1130/G32315.1>, 2011.

605 Limber, P. W., Murray, A. B., Adams, P. N., and Goldstein, E. B.: Unraveling the dynamics that
606 scale cross-shore headland relief on rocky coastlines: 1. Model development, *Journal of*
607 *Geophysical Research: Earth Surface*, 119, 854–873,
608 <https://doi.org/10.1002/2013JF002950>.Received, 2014.

609 Palermo, R. V., Piliouras, A., Swanson, T. E., Ashton, A. D., and Mohrig, D.: The effects of
610 storms and a transient sandy veneer on the interannual planform evolution of a low-relief
611 coastal cliff and shore platform at Sargent Beach, Texas, USA, *Earth Surf. Dynam.*, 9,
612 1111–1123, <https://doi.org/10.5194/esurf-9-1111-2021>, 2021.

613 Palermo, R.V., Perron, J.T., Soderblom, J.M., Birch, S.P.D., Hayes, A.G., Ashton, A.D.,
614 Numerical model of coastal Erosion by Waves and Transgressive Scarps (NEWTS)
615 Version 1.0: U.S. Geological Survey software release,
616 <https://doi.org/10.5066/P9Q6GDGP>, 2023.

617 Perron, J. T., Dietrich, W. E., and Kirchner, J. W.: Controls on the spacing of first-order valleys,
618 *Journal of Geophysical Research: Earth Surface*, 113, 1–21,
619 <https://doi.org/10.1029/2007JF000977>, 2008.

620 Perron, J. T., Kirchner, J. W., and Dietrich, W. E.: Formation of evenly spaced ridges and
621 valleys, *Nature*, 460, 502–505, <https://doi.org/10.1038/nature08174>, 2009.

622 Perron, J. T., Richardson, P. W., Ferrier, K. L., and LapÔtre, M.: The root of branching river
623 networks, *Nature*, 492, 100–103, <https://doi.org/10.1038/nature11672>, 2012.

624 Ranasinghe, R.: On the need for a new generation of coastal change models for the 21st century,
625 *Sci Rep*, 10, 2010, <https://doi.org/10.1038/s41598-020-58376-x>, 2020.

626 Robinson, L. A.: Marine erosive processes at the cliff foot, *Marine Geology*, 23, 257–271,
627 [https://doi.org/10.1016/0025-3227\(77\)90022-6](https://doi.org/10.1016/0025-3227(77)90022-6), 1977.

628 Sunamura, T.: Feedback Relationship in Wave Erosion of Laboratory Rocky Coast, *The Journal*
629 *of Geology*, 84, 427–437, 1976.

630 Sunamura, T.: Geomorphology of rocky coasts, Wiley, 1992.
631 Sunamura, T.: A fundamental equation for describing the rate of bedrock erosion by sediment-
632 laden fluid flows in fluvial, coastal, and aeolian environments, *Earth Surface Processes*
633 *and Landforms*, 43, 3022–3041, <https://doi.org/10.1002/esp.4467>, 2018.
634 Trenhaile, A.: Rocky coasts — their role as depositional environments, *Earth-Science Reviews*,
635 159, 1–13, <https://doi.org/10.1016/j.earscirev.2016.05.001>, 2016.
636 Trenhaile, A. S.: *The geomorphology of rock coasts*, (No Title), 1987.
637 Trenhaile, A. S.: Rock coasts, with particular emphasis on shore platforms, *Geomorphology*, 48,
638 7–22, [https://doi.org/10.1016/S0169-555X\(02\)00173-3](https://doi.org/10.1016/S0169-555X(02)00173-3), 2002.
639 Trenhaile, A. S.: Coastal notches: Their morphology, formation, and function, *Earth-Science*
640 *Reviews*, 150, 285–304, <https://doi.org/10.1016/j.earscirev.2015.08.003>, 2015.
641 Trenhaile, A. S.: *Modeling the Effect of Weathering on the Evolution and Morphology of Shore*
642 *Platforms*, 2024.
643 Walkden, M. J. A. and Hall, J. W.: A predictive Mesoscale model of the erosion and profile
644 development of soft rock shores, *Coastal Engineering*, 52, 535–563,
645 <https://doi.org/10.1016/j.coastaleng.2005.02.005>, 2005.
646 Young, A. P., Flick, R. E., O’Reilly, W. C., Chadwick, D. B., Crampton, W. C., and Helly, J. J.:
647 Estimating cliff retreat in southern California considering sea level rise using a sand
648 balance approach, *Marine Geology*, 348, 15–26,
649 <https://doi.org/10.1016/j.margeo.2013.11.007>, 2014.
650